Title
Carboxyl functionalization of ultrasmall luminescent silicon nanoparticles through thermal hydrosilylation

Journal
Journal of Materials Chemistry, 16(15)

ISSN
0959-9428

Authors
Rogozhina, Elena V
Eckhoff, Dean A
Gratton, Enrico
et al.

Publication Date
2006

DOI
10.1039/b509868h

Carboxyl functionalization of ultrasmall luminescent silicon nanoparticles through thermal hydrosilylation

Elena V. Rogozhina,†[a] Dean A. Eckhoff,†*[b] Enrico Gratton[b] and Paul V. Braun[a]

Received 12th July 2005, Accepted 13th January 2006
First published as an Advance Article on the web 25th January 2006
DOI: 10.1039/b509868h

Functionalization of ultrasmall semiconductor nanoparticles to develop new luminescent probes that are optically bright, stable in aqueous environments, and sized comparably to small organic fluorophores would be of considerable utility for myriad applications in biology. Here, we report one of the first examples of thermal hydrosilylation between a bi-functional alkene and ultrasmall ($\sim$1 nm) H-passivated silicon nanoparticles (Si-np-H) to prepare strongly luminescent, water stable, carboxyl functionalized nanoparticles (Si-np-COOH). Nuclear magnetic resonance, infrared absorption spectroscopy (FTIR), size exclusion chromatography (SEC), and photoluminescence spectroscopy are used to characterize the Si-np dispersions. Based on the SEC and FTIR data, a reaction scheme is proposed to account for side products formed through a free radical cross-linking mechanism. The Si-np-COOH may find use in applications such as biomolecular labeling and biological imaging.

Introduction

Semiconductor nanoparticles exhibit many unique properties not found in the corresponding bulk materials. For example, bulk semiconductors typically have only weak photoluminescence (PL), while semiconductor nanoparticles can have PL quantum yields comparable to organic fluorophores and optical brightnesses an order of magnitude greater.[1–3] They have potential for use in optical and electronic systems[4–7] and biological applications,[1,8–15] in part due to the ability to control their properties by varying the size of the semiconductor core.[3,16–18] Group II–VI nanoparticles such as CdSe and ZnS have received particular interest as bright and photostable markers for biological systems.[1,14–16] They are available in a range of colors and functionalities using the 'core–shell' and 'core–shell–coat' synthetic motifs (*e.g.* CdSe–ZnS–silane nanoparticles).[3,10,11,14–16] Shielding of the II–VI semiconductor core is necessary for chemical and physical stabilization of the nanoparticles in polar solvents and helps to minimize problems with toxicity and PL intermittency.[1,13,14,19] Unfortunately, it also requires that the final products are rather large (*ca.* 5 to 15 nm),[3,16] limiting their use mainly to ensemble measurements in cellular mechanics and imaging.[12–15] For the study of molecular scale processes and single molecule dynamics, a smaller and more diverse class of nanoparticles is preferred.

The group IV semiconductors silicon and germanium are a promising alternative. They have considerable potential to bridge some of the gaps between the properties of multi-layered II–VI nanoparticles (*e.g.* bright and photostable, but large and toxic) and those of organic fluorophores (*e.g.* small and diverse, but photolyzable and generally broad emission). Similar to II–VI semiconductors, the electronic and optical properties of silicon nanoparticles (Si-np) are a strong function of size,[17,18] allowing them to be tailored for specific applications such as multi-color imaging. However, unlike the II–VI systems, silicon has a low inherent toxicity[20] and can form strong and stable covalent bonds with organic materials, providing for a much broader range of possible surface chemistries and functionalities.[21,22] Along with their excellent compatibility with Si-based electronics, this makes possible a wide range of applications for Si-np from biological labeling[8] to inorganic–organic hybrid microelectronics.[5,6] In addition, Si-np may find use as environmentally sensitive probes, similar to work that was done with porous silicon and chemical sensing applications,[23–25] and as we recently demonstrated in principle for ultrasmall H-passivated Si-np (Si-np-H) by showing that their PL has a distinct pH dependence after treatment with HCl.[26]

Researchers have developed many routes for preparing organically functionalized Si-np. However, the products have been generally limited to aliphatic surface chemistries stable only in nonpolar organic solvents. For example, alkylated Si-np (Si–C linkage) were synthesized by reduction of chlorosilanes with Na at high pressure and temperature[27] or by reduction of $SiCl_4$ with NaSi,[28] Mg_2Si,[29] or Na naphthalenide,[30] followed by reaction with Grignard or alkyl lithium reagents, and by hydrosilylation of 1-alkenes with Si-np-H.[31–33] Alkoxylated Si-np (Si–O–C linkage) have been prepared by reducing $SiCl_4$ with Zintl salts followed by treatment with alcohol,[34] through thermal decomposition of diphenyl silane (SiH_2Ph_2) in supercritical octanol,[35] and by thermally activated reaction of alcohols with polydisperse (1 to 10 nm) Si-np-H.[36] In a previous work, we reported alkyl functionalization of ultrasmall Si-np-H through chlorination

[a]*Department of Materials Science and Engineering, Beckman Institute for Advanced Science and Technology, and Frederick Seitz Materials Research Laboratory, University of Illinois at Urbana-Champaign, 1304 West Green Street, Urbana, IL, 61801, USA*
[b]*Laboratory for Fluorescence Dynamics and Department of Physics, University of Illinois at Urbana-Champaign, 1110 West Green Street, Urbana, IL, 61801, USA. E-mail: deckhoff@uiuc.edu*
† EVR and DAE contributed equally to this work.

followed by reaction with an alkyl amine, resulting in covalent attachment of alkyl groups through a Si–NH–C linkage.[37] Unfortunately, this route is limited by the chemical instability of the Si–N bond and the chlorinated intermediate. Likewise, the Si–O–C linkage is generally unstable, being subject to reactions such as hydrolysis and cross-linking through Si–O–Si bridges. The Si–C linkage, however, is quite stable and is generally seen as the ideal bond for attachment of organic functionalities to Si surfaces.[21]

In selecting an appropriate functionalization method, it is also critical to consider the size of the nanoparticles to be modified. For ultrasmall Si-np containing only tens to hundreds of Si atoms, any route leading to Si–Si bond cleavage can have an adverse impact on optical properties, potentially even dissolving the particles completely. For example, alkoxylation by thermally activated reaction with alcohols takes place through cleavage of Si–Si bonds with the formation of Si–H and Si–O–C species.[36] This can result in the loss of Si atoms, as was previously observed for porous silicon.[38] Similarly, alkylation with Grignard or alkyl lithium reagents occurs through nucleophilic attack by a carbanion on an electron deficient Si atom, cleaving a Si–Si bond to form Si–C and silyl anion (Si^-) species.[21,22] To generate a highly robust system, it is preferable to minimize reactions such as these that can degrade the Si core and irreversibly quench their PL. As was demonstrated on flat,[39–43] porous,[21,22,44–46] and nanocrystalline [8,31–33] hydride-terminated Si, this can be accomplished through hydrosilylation with 1-alkenes. In this process, the terminal double bond of the organic linker is directly inserted into a Si–H bond to form the Si–C linkage without breaking Si–Si bonds.[21,22]

In this work, we report on hydrosilylation between ultrasmall ($\sim$1 nm) Si-np-H and an ω-functional, 1-alkene to prepare ester and carboxyl functionalized nanoparticles (Si-np-COOX, X = Me or H). Nuclear magnetic resonance (NMR), infrared absorption spectroscopy (FTIR), size exclusion chromatography (SEC), and PL spectroscopy are used to characterize the Si-np dispersions. Based on the SEC and FTIR data, a reaction scheme is proposed to account for the formation of aggregated side products through a free radical cross-linking mechanism. A polarity based separation is used to isolate the carboxylate modified nanoparticles (Si-np-COO^-), which are shown to maintain the strong PL of the Si core, have sizes comparable to small organic fluorophores, and to be stable in polar solutions.

Experimental

Materials

All materials were used as received except THF (Acros), which was distilled over Na, and MeOH (Acros), which was dried over CaH_2 for 24 hours before use in the ester synthesis. 4-Pentenoyl chloride and 1.6 N n-BuLi in hexane were obtained from Aldrich. Heptanes, xylenes (mixture of isomers), diethyl ether, and NaOH were obtained from Fisher. Water was deionized prior to use. The synthesis and properties of H-passivated Si-np (Si-np-H) prepared through HF/H_2O_2 anodization and ultrasonic fractionation of a crystalline Si wafer have been described elsewhere.[17,47,48]

Methyl 4-pentenoate

Synthesis of the ester followed established procedures.[49,50] First, 28.3 mL of 1.6 N n-BuLi in hexane (0.0453 mol) was slowly added to a solution of MeOH (0.0412 mol) in 60 mL of THF. The reaction mixture was refluxed for 20 min and then 5 mL (0.0453 mol) of 4-pentenoyl chloride in 30 mL of THF was added dropwise to the reaction mixture. A precipitate formed immediately. The reaction mixture was refluxed for 20 h. Diethyl ether (30 mL) was added to the mixture and the organic layer was washed three times with saturated aqueous NaCl. The organic layer was then dried with anhydrous magnesium sulfate and concentrated by roto-evaporation (bath temperature 30–45 °C). The concentrated product was passed through silica gel with CH_2Cl_2 as the eluent to remove traces of 4-pentenoic acid. The collected ester fraction was characterized with FTIR and NMR. Methyl 4-pentenoate yield: 30 wt%, ^{1}H NMR (δ 5.84–5.77 (m, 1H), 5.07–4.97 (m, 2H), 3.66 (s, 3H), 2.42–2.34 (s, 4H)), ^{13}C NMR (δ 173.7, 136.8, 115.7, 51.7, 33.5, 29.0).

Functionalization of Si-np

All hydrosilylation reactions were performed under N_2. Functionalization of Si-np with methyl 4-pentenoate was based in part on procedures for thermal hydrosilylation of alkenes on hydride-terminated Si surfaces.[39,40] A colloid dispersion of fresh Si-np-H in xylenes (45 mL) was reacted with the methyl ester (5 mL, 10% by volume) in refluxing solvent (135–140 °C) for 24 h. Excess ester and xylenes were removed under vacuum. The dried particles were redispersed with ultrasonication in MeOH, forming a yellow solution labeled as the ''methyl ester fraction (Si-np-COOMe)''.

Carboxyl functionalized Si-np were then prepared from the methyl ester fraction through base hydrolysis in a water–methanol mixture (3 : 1) with 7.5 wt% NaOH for 1 h. After vacuum evaporation of the reagents, the residue was redispersed in THF by ultrasonication. The THF dispersion was passed through a paper filter (Whatman #1) and the soluble material was collected and labeled as the ''THF fraction (Si-np-COOH)''. The residue left on the filter paper was dissolved in water, resulting in a clear yellow solution. CH_2Cl_2 was added and shaken vigorously to extract any remaining nonpolar material. The water solution was titrated with HCl to pH 4.2 and dried under vacuum. The solid residue was ultrasonically redispersed in THF and filtered to remove NaCl. The soluble material was labeled as the ''H_2O fraction (Si-np-COOH)''.

FTIR

Infrared spectra were recorded using a Nicolet NEXUS 670 FT-IR spectrometer in absorption mode at 4 cm^{-1} resolution; 16 to 32 scans were collected. Background spectra were obtained using a Si(100) wafer or NaCl crystal.

NMR

Standard solution-phase NMR spectra were obtained on a VARIAN UNITY 400; 6 scans for ^{1}H spectra and 64 scans for ^{13}C spectra were collected. Solution-phase nano-probe (0.7 μL)

MASS NMR spectra were obtained on a VARIAN UNITY INOVA 500 equipped with a magic-angle sample-spinning rotor. 2 000 to 4 000 scans were collected.

SEC

THF dispersions of fresh and organically modified Si-np were injected into a Waters Styragel column set (7.8 mm I.D. × 300 mm) of linked HR 4, HR 1, and HR 0.5 columns. The UV detector was set at 365 nm and THF was used as the eluent with a flow rate of 1 mL min^{-1}.

PL

Optical spectra were recorded on a Jobin-Yvon FluoroMax-2 fluorimeter with a Xe arc lamp light source, 4 nm bandpass excitation and emission monochromators, and suitable correction for lamp fluctuations and spectral response.

Results and discussion

Silicon nanoparticle (Si-np) preparation

Preparation of H-passivated Si-np (Si-np-H) through ultrasonic fractionation of anodically etched porous Si was discovered by Sailor and co-workers in 1992.[51] The nanoparticle size distribution was shown to be a strong function of anodization time and electrolyte bath composition.[52] For example, adding the strong oxidizer H_2O_2 to the bath substantially enhances the etching to yield smaller nanoparticles.[17,47,48] When the ratio of H_2O_2 to HF is greater than about 2, the Si surfaces tend toward the monohydride (≡Si–H) passivation[47] and the luminescent Si-np etched from the wafer, presumably trapped within the pores or weakly bound to the matrix and recovered after fractionation of the porous skeleton, come in a discrete set of favored sizes, the smallest of which is ∼1 nm in diameter.[17]

We confirmed the presence of Si–H groups in the nanoparticle preparation using solution-phase nano-probe ^{1}H NMR. Shown in Fig. 1a is the NMR spectrum for the freshly prepared Si-np-H in d_8-THF. The strong signal at 2.64 ppm is assigned to Si–H protons (*e.g.*, see ref. 53) and the six-times less intense peak at 0.1 ppm is attributed to Si–CH_2– protons. Also seen are signals at 0.88 ppm and 1.29 ppm, characteristic of alkyl chain methyl and methylene protons, respectively. There were no significant signals in the spectrum beyond 4 ppm; specifically, there is no aromatic signal between 6.9 and 7 ppm, ruling out possible assignment of the 2.64 ppm peak to aromatic contaminants. The NMR data conclusively demonstrate the presence of Si–H groups in the Si-np-H preparation. However, given the metastability of the hydride termination,[54] it is likely that some amount of surface oxidation and hydrocarbon contamination are present as well. This was previously observed in work with larger Si-np prepared through ultrasonic fractionation of porous silicon and was attributed to small amounts of oxygen and water along with the extreme conditions of ultrasonication.[52] Thus, it is likely that a majority of the Si–H groups in the nanoparticle preparation are lost during the fractionation process.

The relative size and polydispersity (PD) of the Si-np dispersions was monitored using SEC. Fig. 2 shows the SEC

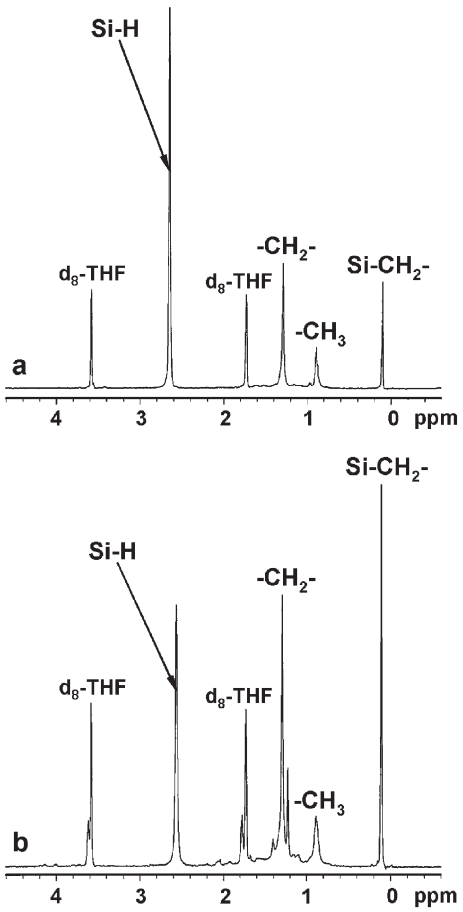

Fig. 1 ^{1}H NMR spectra for: (a) H-passivated Si-np and (b) pentane modified Si-np.

data for freshly prepared and organically modified Si-np. For comparison, the elution profile for a polystyrene standard with M_n = 955 g/mol and PD of 1.1 is shown in Fig. 2a. The standard has a narrow, symmetric peak eluting at 22 min and a smaller peak attributed to trace solvent impurities eluting at 27.5 min. All of the Si-np dispersions (Fig. 2b–f) have elution times between these two points, so it is useful to estimate the corresponding hydrodynamic volumes to use as a rough size calibration of the column. For the polystyrene peak (22 min), we estimate the size using a bulk density ρ ∼1 g/cm^3 and assuming a hydrodynamic volume 25–50% larger than the specific volume (M_n/ρ N_A). This gives a characteristic diameter of ∼1.6 nm for the spherical size-equivalent of the polymer. The solvent impurities peak (27.5 min) consists of small compounds diffusing comparably to the solvent molecules (THF), giving a characteristic size of ∼0.5 nm for this peak.

The SEC profile for the Si-np-H preparation (Fig. 2b) has a single broad peak centered at slightly later retention time (R_V, 23 min) than the standard. The PD can be attributed either to a distribution of Si core sizes or to the formation of aggregated structures between small numbers of individual Si-np. The left half of the peak overlaps with the polystyrene standard, but with significant broadening toward smaller R_V (20–21 min), giving a rough estimate of ∼1.5 to 2 nm for the larger Si structures. The right half of the peak elutes at later R_V

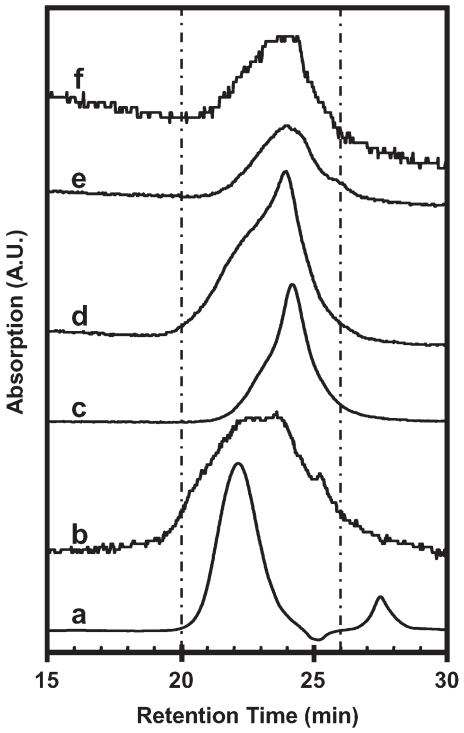

Fig. 2 Size exclusion chromatograms for: (a) polystyrene standard, M_n = 955 Da, PD = 1.1, and (b–f) dispersions of Si-np: (b) H-passivated, (c) aminobutyl modified, (d) methyl ester functionalized, (e) carboxyl functionalized, THF fraction, (f) carboxyl functionalized, H_2O fraction.

(23–26 min), between the polystyrene and solvent impurity peaks of the standard, suggesting sizes of ~1 nm for the smaller Si-np-H. Also shown for comparison are the previously reported SEC data for alkyl amine modified Si-np (Fig. 2c).[37] This sample shows a much narrower peak eluting at later R_V (24 min) with a PD of 1.1, close to that of the standard. The low PD after functionalization is representative of individual, monodisperse Si-np and indicates that either the starting Si-np-H were not irreversibly aggregated or that the larger Si structures were less reactive and removed during purification. Aggregation would not be surprising as untreated Si-np-H were seen to have limited long term stability in common solvents such as THF (the running SEC solvent), xylenes, heptane, chlorobenzene, and acetone, with precipitation evident over months of storage. This process was initially reversible with ultrasonication, but became irreversible over time, perhaps due to formation of Si–O–Si covalent bridges between partially oxidized particles.

The PL properties of the Si-np-H are consistent with a monodisperse population of bright species, further suggesting that aggregation is the more likely cause of size PD in the nanoparticle preparation. Shown in Fig. 3 are a series of PL spectra with excitations ranging from 250–310 nm for the freshly prepared Si-np-H. The PL shows a narrow UV emission with a constant peak wavelength of 305 nm and a FWHM of 0.57 eV (44 nm). The maximum absorption is at 270 nm and the PL drops markedly for excitations of 300 nm or greater. Theoretical modeling of ultrasmall H-passivated Si clusters has demonstrated convincingly that their optical

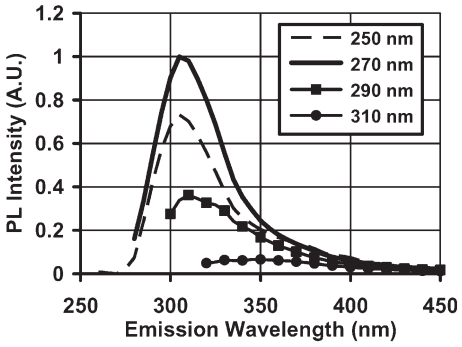

Fig. 3 Photoluminescence spectra for H-passivated Si-np. Excitation at: 250 nm (dashed), 270 nm (solid), 290 nm (squares), 310 nm (circles).

properties are a strong function of particle size.[55–58] Galli and co-workers compared calculations of the optical absorption gap of Si nanoclusters up to 2 nm in diameter using a range of formalisms including quantum Monte Carlo simulations, density functional theory, and empirical pseudopotential methods.[55] For Si clusters ranging in size from 0.5 to 1.5 nm, the results consistently predict a near-linear dependence between the optical gap and Si-np diameter, with the band gap increasing at a rate of ~2 eV nm^{-1} as the cluster size decreases. Given such sensitivity to size, the narrow, constant wavelength peak seen for the Si-np-H (Fig. 3), as opposed to PL that redshifts with the excitation, is representative of a relatively monodisperse population of bright species.

Ester functionalized Si-np

Chemical modification of hydride-terminated Si surfaces has been pursued by many researchers as a route for functionalizing flat and porous Si.[54,59] Hydrosilylation with 1-alkenes is among the more versatile of these, being used for applications such as photopatterning[44] and site-specific ligation of polypeptides.[43] This reaction has several characteristics that make it particularly well-suited for functionalization of ultrasmall Si-np. First, attachment of the organic occurs through the strong and stable Si–C linkage. Second, since it does not cleave Si–Si bonds, hydrosilylation should not degrade the Si core. This is important for the ~1 nm Si-np we are working with, which contain only ~30 Si atoms. Finally, hydrosilylation can be done under relatively mild reaction conditions including thermal activation at 100–150 °C or photo-activation with white light.[21,22] Hydrosilylation is also compatible with bi-functional alkenes using similar protocols, providing a viable route for incorporating a wide range of organic functionalities to the surface of ultrasmall Si-np.

To establish the feasibility of hydrosilylation for our system, we first tested the reaction on the Si-np-H preparation using the simple mono-functional organic 1-pentene. The ^1H NMR spectrum for the resulting pentane modified Si-np is shown in Fig. 1b. It contains the same set of signals seen in the starting material (Fig. 1a), but with the hydrocarbon peaks increasing at the expense of the Si–H peak. After reaction, there is a 4-fold increase in the ratio of signals from Si–CH_2– protons to Si–H protons, showing an increase in Si–C content and indicating successful attachment of pentyl groups to the Si-np

surface. However, since there is still a significant Si–H signal, it is evident that the reaction did not go to completion. This may be caused in part by steric hindrance, with some of the surface area excluded by the added pentyl groups and any pre-existing alkoxy or hydrocarbon contaminants. It should also be noted that liquid-state NMR on colloidal systems can be misleading in that only the more soluble species may be observed. However, our synthetic procedure is designed to remove less soluble species such as large aggregates, so it is preferable that they do not appear in the NMR.

Hydrosilylation with bi-functional alkenes adds additional complexity because of the requirement that the second functional group opposite the alkene is stable to the reaction conditions or can be protected. To meet this requirement, we developed a procedure using methyl 4-pentenoate, a bi-functional organic with a terminal double bond on one end and a methyl ester group on the other. With hydrosilylation, the molecule is attached to the surface through reaction with the terminal double bond, leaving the ester group oriented toward the solvent, ready for further functionalization. Protecting the ester during hydrosilylation is necessary to block unintended nucleophilic reactions between carboxylic acid groups and Si–H species.[39,60] We also tested *tert*-butyl groups as the blocking agent, but found that they were less effective and led to substantial aggregation in the products, presumably due to easier deprotection of the *tert*-butyl group from the ester molecule during reaction. Thus, while the methyl blocking group was seen to be much more effective, deprotection of the ester during hydrosilylation should still be considered as a possible source of side-products.

To characterize the surface chemistry of reaction products, FTIR spectroscopy was used. The spectrum for the methyl ester functionalized nanoparticles (Si-np-COOMe) is shown in Fig. 4b. The ester group shows a strong C=O stretching at 1745 cm^{-1}, very similar to the starting methyl 4-pentenoate (Fig. 4a). The set of peaks in the 3000–2800 cm^{-1} range and the peak at 1450 cm^{-1} are attributed to C–H stretching and bending, respectively, of alkanes. These signals are indicative of successful attachment of methyl ester linkers to the surface. Also present are peaks at 3080 cm^{-1} and 1640 cm^{-1} assigned to =C–H and C=C stretching, respectively, of an alkene. These are characteristic of unreacted double bonds, which could be due to backwards attachment of a deprotected ester molecule or, as will be shown later, free radical propagation during hydrosilylation can lead to reaction side products that contain unreacted alkenes on their surface. Absent from the FTIR spectra is the expected signal from Si–H groups at $\sim$2100 cm^{-1}. We suspect that the small amounts of Si–H groups that remain after ultrasonication and functionalization of the Si-np are lost during the drying process. However, the Si–H signal was clearly seen in the NMR data on the Si-np dispersions discussed above.

The size and PD of the reaction products is seen in the SEC profile for the Si-np-COOMe (Fig. 2d). In comparison to the starting material (Fig. 2b), this fraction exhibits a narrow, asymmetric profile weighted toward later R_V, showing that the larger Si structures were preferentially removed from the sample during hydrosilylation. The peak maximum (24 min) coincides with the maximum observed for the alkyl amine modified Si-np (Fig. 2c). However, the broadening toward earlier R_V (shoulder $\sim$22 min) in much more significant after hydrosilylation that it was after chlorination–amination.[37] This may be due to particles that were already aggregated prior to reaction since the starting Si-np-H were seen to be polydisperse (Fig. 2b). However, this seems unlikely since comparable broadening is not seen for the alkyl amine modified Si-np, which were synthesized from Si-np-H prepared under the same conditions. Thus, we hypothesize that the broadening is due, at least in part, to side products formed during hydrosilylation. Later in this report, we will propose a reaction scheme, consistent with the SEC and FTIR data, that suggests aggregates of modified particles can form through an

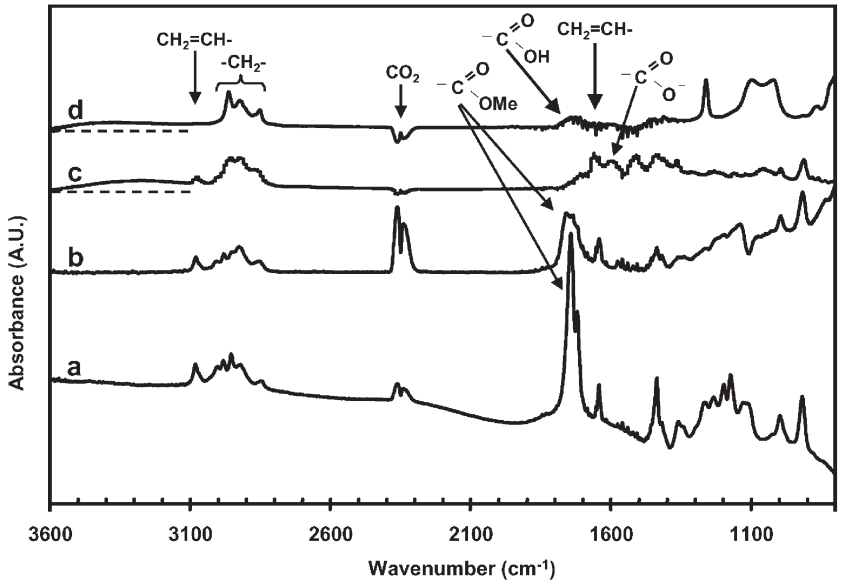

Fig. 4 FTIR absorption spectra for: (a) methyl 4-pentenoate and (b–d) dried films of Si-np; (b) methyl ester functionalized, (c) carboxyl functionalized, THF fraction, (d) carboxyl functionalized, H_2O fraction.

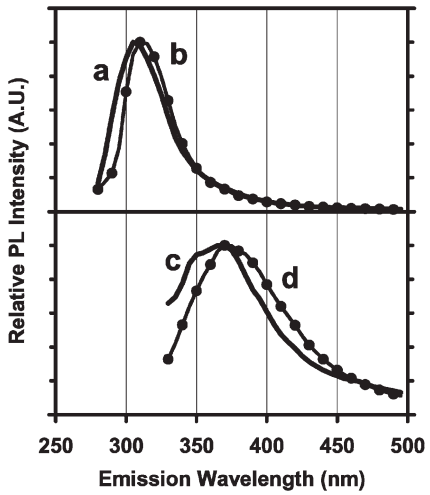

Fig. 5 Photoluminescence spectra for H-passivated Si-np (solid) and methyl ester functionalized Si-np (circles). Excitation at: (a,b) 270 nm, (c,d) 320 nm.

interparticle free radical cross-linking mechanism during functionalization.

Hydrosilylation had only relatively minor effects on the PL of the Si-np. Fig. 5 compares two sets of PL spectra for the nanoparticles before (solid line) and after (circles) ester functionalization. The strongest PL occurs with 270 nm excitation (Fig. 5a,b). The peak emission for the Si-np-COOMe is at 310 nm, redshifted 5 nm relative to the starting material, and the FWHM decreases from 0.57 eV before reaction to 0.48 eV afterwards. It appears that this narrowing occurs mainly on the blue-edge of the peak. For 320 nm excitation (Fig. 5c,d), the PL is considerably weaker, with a 22-fold reduction in peak intensity for the Si-np-H and an 18-fold decrease for the Si-np-COOMe relative to 270 nm excitation. The PL maximum is at 370–375 nm, again slightly redshifted after functionalization. Also note that the Si-np-H spectrum (Fig. 5c) shows a small peak or shoulder at about 340–350 nm, which is not seen in the Si-np-COOMe spectrum (Fig. 5d), again showing that some amount of quenching occurs on the blue-edge of the PL peaks during hydrosilylation.

Carboxyl functionalized Si-np

Carboxyl functionalized nanoparticles (Si-np-COOH) were prepared through base hydrolysis of the Si-np-COOMe. Separation of the products based on their polarity was done through consecutive THF extractions of the sample dried at basic and acidic conditions to yield the ''THF fraction'' and the ''H_2O fraction'', respectively. The THF fraction was obtained from the basified solids in which the carboxyl groups are ionized. Thus, it should contain the less polar products like unmodified Si-np, neutral oxidized material, and nanoparticles with allyl surface groups, $–CH(–CH_2–COO^-)–CH=CH_2$, formed through the free radical mechanism described below. The H_2O fraction should then contain the more polar Si-np that were not soluble in THF under basic conditions; specifically, the Si-np that have a significant amount of carboxylic acid functionality and a negligible amount of allyl groups on their surface (*i.e.* the desired product).

As an initial indication of successful derivatization, in contrast to the Si-np-H, the carboxyl modified Si-np were insoluble in heptane, but formed stable solutions in polar solvents such as methanol or basic water. Physical confirmation was also evident with the behavior of the Si-np-COOH in aqueous solutions. Titration with HCl turned the solution cloudy when the pH was reduced below about 5; transparency returned upon increasing the pH above 5 with NaOH. This process was reversible many times. Such pH sensitive aggregation can explained by the presence of –COOH groups on the nanoparticle surface, which have a pK_a of about 5.[61] Below this pH, the carboxyl groups are protonated, participate in H-bonding, and are much less hydrophilic, resulting in aggregate formation. When the pH is increased, the carboxyl groups deprotonate and charge repulsion disperses the aggregates.

FTIR analysis of the THF and H_2O fractions demonstrates successful partitioning of reaction products based on polarity. The FTIR spectrum of the THF fraction (Fig. 4c) displays C=O stretching at 1600 cm^{-1} characteristic of the carboxylate anion ($–COO^-$), a broad peak centered $\sim$3250 cm^{-1} suggestive of oxidation, and signals characteristic of unreacted alkene groups with =C–H stretching at 3080 cm^{-1} and C=C stretching at 1640 cm^{-1}. The FTIR spectrum of the H_2O fraction (Fig. 4d) shows C=O stretching at 1745 cm^{-1} attributed to carboxyl groups (–COOH) and a broad, low intensity O–H stretching band centered $\sim$3350 cm^{-1}. Note the absence of signals from unreacted alkene groups for this fraction, demonstrating successful removal of these side products from the sample. The nanoparticle size distribution for the THF and H_2O fractions is shown by the SEC data in Fig. 2e,f. Both fractions were characterized by a single, asymmetric peak having lower PD than the Si-np-COOMe before hydrolysis (Fig. 2d). The elution maximum of the THF fraction (Fig. 2e) had the same value as that for the Si-np-COOMe (24 min) and the broadening toward earlier R_V was less pronounced. The maximum of the H_2O fraction (Fig. 2f) was shifted a tiny amount to earlier R_V and the broadening was comparable to that for the THF fraction.

Unlike hydrosilylation, base hydrolysis of the methyl ester has a substantive effect on the PL of the Si-np-COOH dispersions. Fig. 6 compares two sets of PL spectra for the THF fraction (solid line) and H_2O fraction (circles). For 270 nm excitation, the H_2O fraction (Fig. 6b) has nearly identical PL to the Si-np-COOMe (Fig. 5b) and Si-np-H (Fig. 5a). The THF fraction, however, shows a sizable increase in PL at longer wavelengths from $\sim$330–450 nm (Fig. 6a). Theoretical modeling of ultrasmall Si clusters suggests that redshifted luminescence may be caused by oxidation of the Si-np surface.[56,57] In a recent work, we reported similar, but much more substantial increases in redshifted PL after treatment of unmodified Si-np-H with NaOH under nearly identical conditions to the base hydrolysis.[26] The results were attributed to oxidation of the nanoparticle surface with possible formation of Si–O–Si bridge structures. Note that the relative lack of redshifted PL for the H_2O fraction suggests that the carboxyl modification provides some additional protection against surface oxidation.

An increase in redshifted PL for the THF fraction is also evident by comparing the relative magnitudes of the PL for

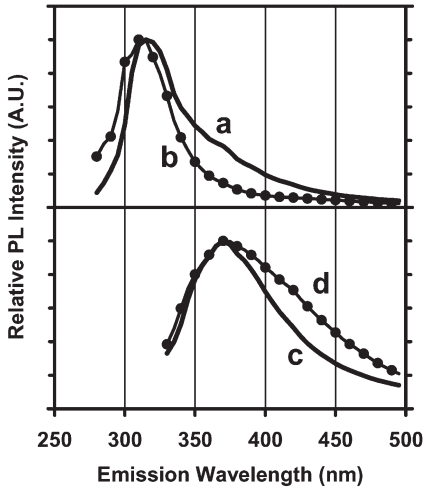

Fig. 6 Photoluminescence spectra for carboxylate functionalized Si-np; THF fraction (solid) and H_2O fraction (circles). Excitation at: (a,b) 270 nm, (c,d) 320 nm.

270 nm and 320 nm excitation. For the THF fraction, the PL intensity is only about 5-fold smaller for the longer wavelength excitation; whereas, for the Si-np-H, Si-np-COOMe, and H_2O fractions, this ratio is 22, 18, and 19 times smaller, respectively. Finally, when comparing the PL spectra for 320 nm excitation, both the THF fraction (Fig. 6c) and H_2O fraction (Fig. 6d) show the same PL maximum at 370–375 nm that was seen in the Si-np-H (Fig. 5c) and the Si-np-COOMe (Fig. 5d). However, it appears that the H_2O fraction has an additional component emitting at $\sim$425 nm, which was not seen clearly in the spectrum for the THF fraction.

Hydrosilylation mechanism

Based on the SEC and FTIR data, we suggest the following mechanism for functionalization of the Si-np (Scheme 1). (i) *Activation*: **2**, a nanoparticle containing a silyl radical forms through thermally activated homolytic cleavage of a Si–H bond on **1** (reaction a). (ii) *Capping*: through reaction b, **2** reacts with an alkene molecule covalently attaching it to the surface with formation of **3**. (iii) *Propagation*: the radical on **3** can be transferred by abstracting hydrogen from a nearby Si–H bond (reaction c) or from **1** forming a new silyl radical on **2** (reaction d) or by abstracting the α-hydrogen from an alkene molecule forming **4** (reaction e). (iv) *Combination*: the silyl and alkyl radicals on **2** and **3** can combine resulting in cross-linked particles **5**, **6**, and **7** (reactions f–h). Additionally, combination of radicals on **2** or **3** with **4** generates particles with double bonds (**8** and **9**, reactions i–j).

Thus, thermal hydrosilylation of alkenes in colloid dispersions of Si-np-H can result in isolated alkylated particles (**1**), particles with allyl fragments on their surface (**8** and **9**), and aggregates of cross-linked particles (**5**, **6**, and **7**). The FTIR analysis clearly shows that double bonds are present in the Si-np-COOMe (Fig. 4b), consistent with formation of side products **8** and **9**. The SEC analysis shows a substantial broadening toward earlier R_V (*i.e.* larger structures) in the Si-np-COOMe (Fig. 2d) compared to alkyl amine modified

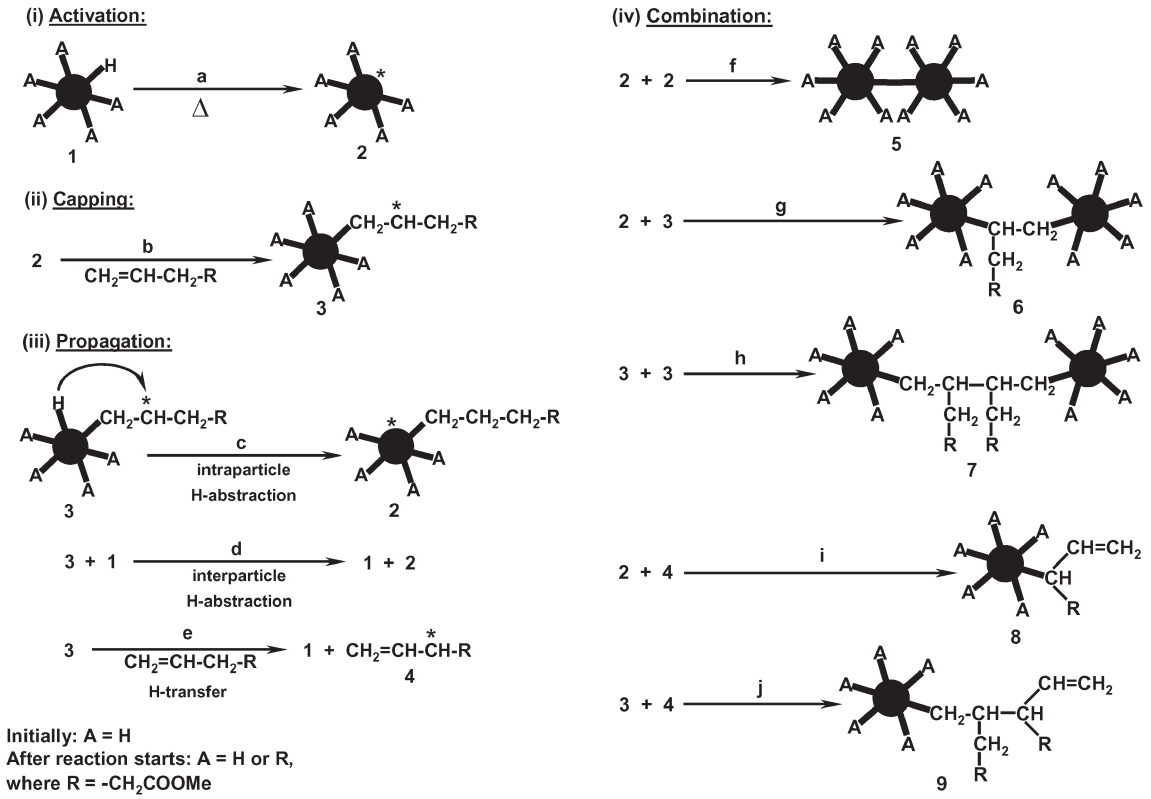

Scheme 1 Reaction mechanism for hydrosilylation of H-passivated Si-np.

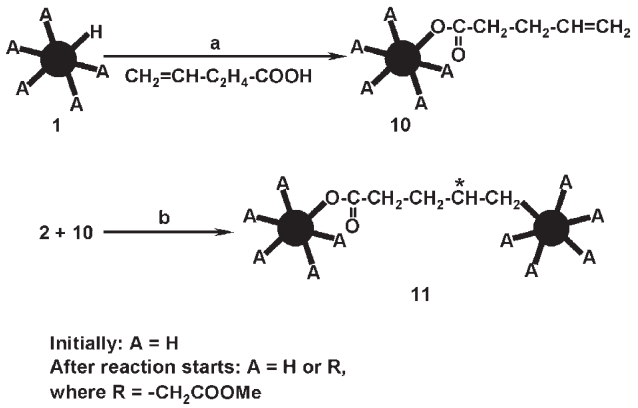

Scheme 2 Cross-linking mechanism due to deprotected ester during hydrosilylation.

Si-np (Fig. 2c), consistent with formation of cross-linked products **5**, **6**, and **7**.

During hydrosilylation of the bi-functional methyl ester, thermal decomposition of the ester can also occur, generating a reactive acid group.[39,60] This provides another route (Scheme 2) through which cross-linking of nanoparticles can occur. Si–O–C bonds are first formed through reaction of a Si–H bond with the acid group (reaction a), introducing double bonds on the surface of **10**. The alkene then reacts with silyl radicals (**2**), cross-linking the particles (reaction b). Once aggregated, the probability of interparticle radical combination (Scheme 1, reactions f–h) increases. Additionally, alkyl radicals on aggregates (**11**) resulting from hydrosilylation of a double bond on **10** may participate in radical propagation and combination (Scheme 1, steps iii and iv, respectively). The silyl ester groups are partially decomposed by NaOH during hydrolysis of the methyl ester groups. Evidence for this is seen in the SEC data, where the broadening toward earlier R_V is significantly reduced after hydrolysis (Fig. 2e,f).

To study the effect of ester concentration, hydrosilylation was also performed with half the concentration of methyl ester (5 vol%). The FTIR spectrum of this sample shows only residual C–H stretching of double bonds and the SEC size distribution was shifted toward earlier R_V (data not shown). This demonstrates that lower concentration of the bi-functional alkene increases the fraction of aggregated particles and decreases the presence of allyl fragments on the surface. The lower concentration of methyl ester reduces the rate of reaction of silyl radicals on **2** with alkene molecules (Scheme 1, reaction b) and the formation of **4** (reaction e), as both are first order with respect to alkene concentration. This decreases the rate of formation of isolated particles with saturated and allyl fragments on their surface through reactions c–e and i,j of Scheme 1, respectively. However, the rate of combination between particles (reactions f–h) should not change, thus explaining the increase in average aggregate size.

Conclusions

A versatile route for chemical functionalization of ultrasmall Si-np based on thermally activated hydrosilylation of bi-functional alkenes with H-passivated Si surfaces was developed to synthesize ester and carboxyl functionalized nanoparticles (Si-np-COOX, X = Me or H). SEC and FTIR characterization suggested that nanoparticle aggregation during functionalization is driven by free radical propagation and a reaction mechanism was proposed to account for the formation of cross-linked side products. The analysis also showed that side products with unreacted double bonds on their surface, as well as oxidized material created during base hydrolysis, can be removed from the samples using polarity based separations.

The Si-np-COOH were shown to preserve the strong PL of the Si core, have sizes comparable to small organic fluorophores, and to be stable in polar solutions. The ester/carboxyl functionality can also serve as a facile substrate for biomolecular attachment through its reaction with primary amines, making possible myriad applications as a biological marker. In a future publication,[62] we will report on our work using capillary electrophoresis with on-column PL detection to separate and analyze the carboxylate functionalized nanoparticles (Si-np-COO^-). Further research will focus on several issues that must be resolved before this material can receive significant use as a biological marker.

Acknowledgements

The authors thank Dr M. Nayfeh for providing the Si material used in this study. We are appreciative of support from: Motorola, the National Science Foundation (NSEC program DMR-0117792 and BES-0118053), the National Institutes for Health (institutional NRSA in molecular biophysics 5T32GM08276 and PHS 5 P41-RRO3155), and the U.S. Department of Energy, Division of Materials Sciences, under Award No. DEFG02-91-ER45439, through the Frederick Seitz Materials Research Laboratory at the University of Illinois at Urbana-Champaign.

References

1 D. R. Larson, W. R. Zipfel, R. M. Williams, S. W. Clark, M. P. Bruchez, F. W. Wise and W. W. Webb, Water-soluble quantum dots for multiphoton fluorescence imaging in vivo, *Science*, 2003, **300**, 1434.
2 M. A. Hines and P. Guyot-Sionnest, Bright UV–blue luminescent colloidal ZnSe nanocrystals, *J. Phys. Chem. B*, 1998, **102**, 3655.
3 B. O. Dabbousi, J. Rodriguez-Viejo, F. V. Mikulec, J. R. Heine, H. Mattoussi, R. Ober, K. F. Jensen and M. G. Bawendi, (CdSe)ZnS core–shell quantum dots: Synthesis and characterization of a size series of highly luminescent nanocrystallites, *J. Phys. Chem. B*, 1997, **101**, 9463.
4 D. L. Feldheim and C. D. Keating, Self-assembly of single electron transistors and related devices, *Chem. Soc. Rev.*, 1998, **27**, 1.
5 Z. Ding, B. M. Quinn, S. K. Haram, L. E. Pell, B. A. Korgel and A. J. Bard, Electrochemistry and electrogenerated chemiluminescence from silicon nanocrystal quantum dots, *Science*, 2002, **296**, 1293.
6 B. Sweryda-Krawiec, T. Cassagneau and J. H. Fendler, Ultrathin electroactive junctions assembled from silicon nanocrystallites and polypyrrole, *Adv. Mater.*, 1999, **11**, 659.
7 L. Pavesi, L. Dal Negro, C. Mazzoleni, G. Franzò and F. Priolo, Optical gain in silicon nanocrystals, *Nature*, 2000, **408**, 440.
8 L. Wang, V. Reipa and J. Blasic, Silicon nanoparticles as a luminescent label to DNA, *Bioconjugate Chem.*, 2004, **15**, 409.

9 D. Gerion, W. J. Parak, S. C. Williams, D. Zanchet, C. M. Micheel and A. P. Alivisatos, Sorting fluorescent nanocrystals with DNA, *J. Am. Chem. Soc.*, 2002, **124**, 7070.
10 W. J. Parak, D. Gerion, D. Zanchet, A. S. Woerz, T. Pellegrino, C. Micheel, S. C. Williams, M. Seitz, R. E. Bruehl, Z. Bryant, C. Bustamante, C. R. Bertozzi and A. P. Alivisatos, Conjugation of DNA to silanized colloidal semiconductor nanocrystalline quantum dots, *Chem. Mater.*, 2002, **14**, 2113.
11 H. Mattoussi, J. M. Mauro, E. R. Goldman, G. P. Anderson, V. C. Sundar, F. V. Mikulec and M. G. Bawendi, Self-assembly of CdSe–ZnS quantum dot bioconjugates using an engineered recombinant protein, *J. Am. Chem. Soc.*, 2000, **122**, 12142.
12 P. Alivisatos, The use of nanocrystals in biological detection, *Nat. Biotechnol.*, 2004, **22**, 47.
13 X. Michalet, F. F. Pinaud, L. A. Bentolila, J. M. Tsay, S. Doose, J. J. Li, G. Sundaresan, A. M. Wu, S. S. Gambhir and S. Weiss, Quantum dots for live cells, in vivo imaging, and diagnostics, *Science*, 2005, **307**, 538.
14 B. Dubertret, P. Skourides, D. J. Norris, V. Noireaux, A. H. Brivanlou and A. Libchaber, In vivo imaging of quantum dots encapsulated in phospholipid micelles, *Science*, 2002, **298**, 1759.
15 W. C. W. Chan and S. Nie, Quantum dot bioconjugates for ultrasensitive nonisotopic detection, *Science*, 1998, **281**, 2016.
16 D. Gerion, F. Pinaud, S. C. Williams, W. J. Parak, D. Zanchet, S. Weiss and A. P. Alivisatos, Synthesis and properties of biocompatible water-soluble silica-coated CdSe/ZnS semiconductor quantum dots, *J. Phys. Chem. B*, 2001, **105**, 8861.
17 G. Belomoin, J. Therrien, A. Smith, S. Rao, R. Twesten, S. Chaieb, M. H. Nayfeh, L. Wagner and L. Mitas, Observation of a magic discrete family of ultrabright Si nanoparticles, *Appl. Phys. Lett.*, 2002, **80**, 841.
18 G. Ledoux, O. Guillois, D. Porterat, C. Reynaud, F. Huisken, B. Kohn and V. Paillard, Photoluminescence properties of silicon nanocrystals as a function of their size, *Phys. Rev. B*, 2000, **62**, 15942.
19 M. Nirmal, B. O. Dabbousi, M. G. Bawendi, J. J. Macklin, J. K. Trautman, T. D. Harris and L. E. Brus, Fluorescence intermittency in single cadmium selenide nanocrystals, *Nature*, 1996, **383**, 802.
20 A. H. Mayne, S. C. Bayliss, P. Barr, M. Tobin and L. D. Buckberry, Biologically interfaced porous silicon devices, *Phys. Status Solidi A*, 2000, **182**, 505.
21 M. P. Stewart and J. M. Buriak, New approaches toward the formation of silicon–carbon bonds on porous silicon, *Comments Inorg. Chem.*, 2002, **23**, 179.
22 J. M. Buriak, Organometallic chemistry on silicon surfaces: Formation of functional monolayers bound through Si–C bonds, *Chem. Commun.*, 1999, 1051.
23 J. H. Song and M. J. Sailor, Quenching of photoluminescence from porous silicon by aromatic molecules, *J. Am. Chem. Soc.*, 1997, **119**, 7381.
24 M. T. Kelly and A. B. Bocarsly, Mechanisms of photoluminescent quenching of oxidized porous silicon: Applications to chemical sensing, *Coord. Chem. Rev.*, 1998, **171**, 251.
25 W. J. Jin, G. L. Shen and R. Q. Yu, Organic solvent induced quenching of porous silicon photoluminescence, *Spectrochim. Acta, Part A*, 1998, **54**, 1407.
26 D. A. Eckhoff, J. D. B. Sutin, R. M. Clegg, E. Gratton, E. V. Rogozhina and P. V. Braun, Optical characterization of ultrasmall Si nanoparticles prepared through electrochemical dispersion of bulk Si, *J. Phys. Chem. B*, 2005, **109**, 19786.
27 J. R. Heath, A liquid-solution-phase synthesis of crystalline silicon, *Science*, 1992, **258**, 1131.
28 D. Mayeri, B. L. Phillips, M. P. Augustine and S. M. Kauzlarich, NMR study of the synthesis of alkyl-terminated silicon nanoparticles from the reaction of $SiCl_4$ with the Zintl salt, NaSi, *Chem. Mater.*, 2001, **13**, 765.
29 C. Yang, R. A. Bley, S. M. Kauzlarich, H. W. H. Lee and G. R. Delgado, Synthesis of alkyl-terminated silicon nanoclusters by a solution route, *J. Am. Chem. Soc.*, 1999, **121**, 5191.
30 R. K. Baldwin, K. A. Pettigrew, J. C. Garno, P. P. Power, G. Liu and S. M. Kauzlarich, Room temperature solution synthesis of alkyl-capped tetrahedral shaped silicon nanocrystals, *J. Am. Chem. Soc.*, 2002, **124**, 1150.
31 L. H. Lie, M. Duerdin, E. M. Tuite, A. Houlton and B. R. Horrocks, Preparation and characterisation of luminescent alkylated-silicon quantum dots, *J. Electroanal. Chem.*, 2002, **538–539**, 183.
32 W. D. Kirkey, Y. Sahoo, X. Li, Y. He, M. T. Swihart, A. N. Cartwright, S. Bruckenstein and P. N. Prasad, Quasi-reversible photoluminescence quenching of stable dispersions of silicon nanoparticles, *J. Mater. Chem.*, 2005, **15**, 2028.
33 R. D. Tilley, J. H. Warner, K. Yamamoto, I. Matsui and H. Fujimori, Micro-emulsion synthesis of monodisperse surface stabilized silicon nanocrystals, *Chem. Commun.*, 2005, 1833.
34 R. A. Bley and S. M. Kauzlarich, A low-temperature solution phase route for the synthesis of silicon nanoclusters, *J. Am. Chem. Soc.*, 1996, **118**, 12461.
35 J. D. Holmes, K. J. Ziegler, R. C. Doty, L. E. Pell, K. P. Johnston and B. A. Korgel, Highly luminescent silicon nanocrystals with discrete optical transitions, *J. Am. Chem. Soc.*, 2001, **123**, 3743.
36 B. Sweryda-Krawiec, T. Cassagneau and J. H. Fendler, Surface modification of silicon nanocrystallites by alcohols, *J. Phys. Chem. B*, 1999, **103**, 9524.
37 E. Rogozhina, G. Belomoin, A. Smith, L. Abuhassan, N. Barry, O. Akcakir, P. V. Braun and M. H. Nayfeh, Si–N linkage in ultrabright, ultrasmall Si nanoparticles, *Appl. Phys. Lett.*, 2001, **78**, 3711.
38 N. Y. Kim and P. E. Laibinis, Thermal derivatization of porous silicon with alcohols, *J. Am. Chem. Soc.*, 1997, **119**, 2297.
39 A. B. Sieval, A. L. Demirel, J. W. M. Nissink, M. R. Linford, J. H. van der Maas, W. H. de Jeu, H. Zuilhof and E. J. R. Sudhölter, Highly stable Si–C linked functionalized monolayers on the silicon (100) surface, *Langmuir*, 1998, **14**, 1759.
40 A. B. Sieval, R. Linke, H. Zuilhof and E. J. R. Sudhölter, High quality alkyl monolayers on silicon surfaces, *Adv. Mater.*, 2000, **12**, 1457.
41 M. R. Linford, P. Fenter, P. M. Eisenberger and C. E. D. Chidsey, Alkyl monolayers on silicon prepared from 1-alkenes and hydrogen-terminated silicon, *J. Am. Chem. Soc.*, 1995, **117**, 3145.
42 T. Böcking, M. James, H. G. L. Coster, T. C. Chilcott and K. D. Barrow, Structural characterization of organic multilayers on silicon (111) formed by immobilization of molecular films on functionalized Si–C linked monolayers, *Langmuir*, 2004, **20**, 9227.
43 Y. Coffinier, C. Olivier, A. Perzyna, B. Grandidier, X. Wallart, J. O. Durand, O. Melnyk and D. Stiévenard, Semicarbazide-functionalized Si(111) surfaces for the site-specific immobilization of peptides, *Langmuir*, 2005, **21**, 1489.
44 M. P. Stewart and J. M. Buriak, Exciton-mediated hydrosilylation on photoluminescent nanocrystalline silicon, *J. Am. Chem. Soc.*, 2001, **123**, 7821.
45 J. M. Schmeltzer, L. A. Porter, Jr., M. P. Stewart and J. M. Buriak, Hydride abstraction initiated hydrosilylation of terminal alkenes and alkynes on porous silicon, *Langmuir*, 2002, **18**, 2971.
46 R. Boukherroub, J. T. C. Wojtyk, D. D. M. Wayner and D. J. Lockwood, Thermal hydrosilylation of undecylenic acid with porous silicon, *J. Electrochem. Soc.*, 2002, **149**, H59.
47 Z. Yamani, W. H. Thompson, L. AbuHassan and M. H. Nayfeh, Ideal anodization of silicon, *Appl. Phys. Lett.*, 1997, **70**, 3404.
48 O. Akcakir, J. Therrien, G. Belomoin, N. Barry, J. D. Muller, E. Gratton and M. Nayfeh, Detection of luminescent single ultrasmall silicon nanoparticles using fluctuation correlation spectroscopy, *Appl. Phys. Lett.*, 2000, **76**, 1857.
49 G. P. Crowther, E. M. Kaiser, R. A. Woodruff and C. R. Hauser, Esterification of hindered alcohols, *Org. Synth.*, 1988, **Coll. Vol. 6**, 259.
50 E. M. Kaiser and R. A. Woodruff, Synthesis of estersof acid-unstable alcohols by means of n-butyllithium, *J. Org. Chem.*, 1970, **35**, 1198.
51 J. L. Heinrich, C. L. Curtis, G. M. Credo, K. L. Kavanagh and M. J. Sailor, Luminescent colloidal silicon suspensions from porous silicon, *Science*, 1992, **255**, 66.
52 R. A. Bley, S. M. Kauzlarich, J. E. Davis and H. W. H. Lee, Characterization of silicon nanoparticles prepared from porous silicon, *Chem. Mater.*, 1996, **8**, 1881.
53 E. A. Williams, NMR spectroscopy of organosilicon compounds, in *The Chemistry of Organic Silicon Compounds*, ed. S. Patai and

Z. Rappoport, John Wiley & Sons Ltd., New York, 1989, ch. 8, p. 515.
54 J. M. Buriak, Organometallic chemistry on silicon and germanium surfaces, *Chem. Rev.*, 2002, **102**, 1271.
55 A. J. Williamson, J. C. Grossman, R. Q. Hood, A. Puzder and G. Galli, Quantum Monte Carlo calculations of nanostructure optical gaps: Application to silicon quantum dots, *Phys. Rev. Lett.*, 2002, **89**, 196803.
56 A. Puzder, A. J. Williamson, J. C. Grossman and G. Galli, Surface control of optical properties in silicon nanoclusters, *J. Chem. Phys.*, 2002, **117**, 6721.
57 I. Vasiliev, J. R. Chelikowsky and R. M. Martin, Surface oxidation effects on the optical properties of silicon nanocrystals, *Phys. Rev. B*, 2002, **65**, 121302.
58 C. Delerue, M. Lannoo and G. Allan, Excitonic and quasi-particle gaps in Si nanocrystals, *Phys. Rev. Lett.*, 2000, **84**, 2457.
59 M. J. Sailor and E. J. Lee, Surface chemistry of luminescent silicon nanocrystallites, *Adv. Mater.*, 1997, **9**, 783.
60 T. Bitzer, T. Alkunshalie and N. V. Richardson, An HREELS investigation of the adsorption of benzoic acid and aniline on Si(100)-2 × 1, *Surf. Sci.*, 1996, **368**, 202.
61 A. J. Streitwieser and C. H. Heathcock, in *Introduction to Organic Chemistry*, Macmillan Publishing Co., New York, 1981, pp. 501–505.
62 D. A. Eckhoff, J. N. Stuart, J. D. B. Sutin, J. V. Sweedler and E. Gratton, *Capillary electrophoresis of ultrasmall carboxylate functionalized silicon nanoparticles*, unpublished work.